American Mineralogist, Volume 77, pages 1275–1284, 1992

Walthierite, $Ba_{0.5}\square_{0.5}Al_3(SO_4)_2(OH)_6$, and huangite, $Ca_{0.5}\square_{0.5}Al_3(SO_4)_2(OH)_6$, two new minerals of the alunite group from the Coquimbo region, Chile

Gejing Li, Donald R. Peacor, Eric J. Essene
Department of Geological Sciences, University of Michigan, Ann Arbor, Michigan 48109-1063, U.S.A.
David R. Brosnahan
LAC Minerals (USA), Inc., 8925 East Nichols Avenue, Englewood, Colorado 80112-3410, U.S.A.
Richard E. Beane
1761 East Deer Hollow Loop, Oro Valley, Arizona 85737, U.S.A.

Abstract

Walthierite and huangite, two new members of the alunite group, were found in the Tambo mining district and the El Indio gold, silver, and copper deposit, Coquimbo region, Chile, respectively. Walthierite, $Ba_{0.5}\square_{0.5}Al_3(SO_4)_2(OH)_6$, is associated with alunite, jarosite, barite, quartz, and pyrite in veins. Huangite, $Ca_{0.5}\square_{0.5}Al_3(SO_4)_2(OH)_6$, coexists with kaolinite, pyrite, and woodhouseite in altered wall rocks. The new alunite group minerals have space group $R\bar{3}m$, $Z = 6$, with lattice parameters $a = 6.992(4)$ Å, $c = 34.443(8)$ Å, $D_{calc} = 3.02$ g/cm³ for walthierite, and $a = 6.983(5)$ Å, $c = 33.517(9)$ Å, $D_{calc} = 2.80$ g/cm³ for huangite. The strongest lines in the X-ray powder diffraction patterns are (*d, I, hkl*): 5.73,(50),(006); 3.49,(55),(110); 2.98,(100),(116); 2.283,(80),(1,0,14); 1.909,(70),(0,0,18) for walthierite, and 4.91,(75),(014); 2.97,(100),(116); 2.231,(51),(1,0,14); 1.899,(43),(306); 1.375,(40),(3,1,14) for huangite. Both minerals show superlattice reflections with c that is double that of alunite, resulting from the ordering of cations and vacancies on 12-fold coordinated M sites. Both minerals are transparent, white to light yellowish in color, and have perfect {001} cleavage. Optically, they are uniaxial positive with negative elongation. The indices of refraction are $\omega = 1.588(2)$, $\epsilon = 1.604(2)$ for walthierite. Minamiite is now considered to be a Na-dominant and Ca-bearing member, rather than a Ca-dominant end-member of the alunite group; huangite is now considered to be the Ca end-member. Wide miscibility gaps may exist between walthierite and natroalunite and between huangite and alunite. Extensive solid solution probably occurs between walthierite and alunite, huangite and natroalunite, and huangite and woodhouseite. The nature of occurrence and stability relations for walthierite and huangite indicate that they, like other alunite group minerals, are stable only under acid sulfate hydrothermal conditions.

Introduction

The general formula for minerals of the alunite group is $MR_3(SO_4)_2(OH)_6$, where the 12-fold-coordinated M site may be occupied by one- or two-valent ions such as Na^+, K^+, H_3O^+, NH_4^+, Ca^{2+}, Sr^{2+}, Pb^{2+}, or Ba^{2+}, and the octahedrally coordinated R site is usually occupied principally by Al^{3+} or Fe^{3+}. The alunite group consists of approximately 20 trigonal minerals with space group $R\bar{3}m$, having approximate lattice parameters $a = 7$ Å and $c = 17$ Å. However, minerals in the alunite group with divalent cations on M sites, such as plumbojarosite (Szymański, 1985) and minamiite (Ossaka et al., 1982), have a superlattice with c that is double that of alunite. Doubling is caused by ordering of Pb^{2+} and vacancies in M sites in plumbojarosite and by partial ordering of vacancies and some Ca^{2+} substituting for Na^+ in minamiite, $Na_{0.36}Ca_{0.27}K_{0.10}\square_{0.27}Al_3(SO_4)_2(OH)_6$, where $\square$ represents vacancies on the 12-fold-coordinated M site. On the other hand, compounds $M_{0.5}\square_{0.5}Al_3(SO_4)_2(OH)_6$ with M = Ca^{2+} (Ossaka et al., 1987), Pb^{2+}, Sr^{2+}, or Ba^{2+} (Okada et al., 1987) synthesized under hydrothermal conditions have M^{2+}-vacancy ordering, although powder X-ray diffraction (XRD) data of synthetic $Sr_{0.5}\square_{0.5}Al_3(SO_4)_2(OH)_6$ and $Ba_{0.5}\square_{0.5}Al_3(SO_4)_2(OH)_6$ were not obtained. Although syntheses of many compounds with the formula $M_{0.5}\square_{0.5}Al_3(SO_4)_2(OH)_6$ have been reported, no naturally occurring Ba or Ca end-members have been described. In this study, Ba and Ca end-members of the series with $^{[6]}Al^{3+}$ are characterized. The Ba end-member has been named walthierite in recognition of the late Thomas N. Walthier, who played a significant role in the exploration of the El Indio deposit and the Tambo mining district, Coquimbo region, Chile. The Ca end-member has been named huangite in honor of Yunhui Huang, in part for recognition of her contributions to the mineralogical and petrological studies of a contact metamorphic Be-deposit in Hsianghualing, south-central China. Because the name

0003–004X/92/1112–1275$02.00

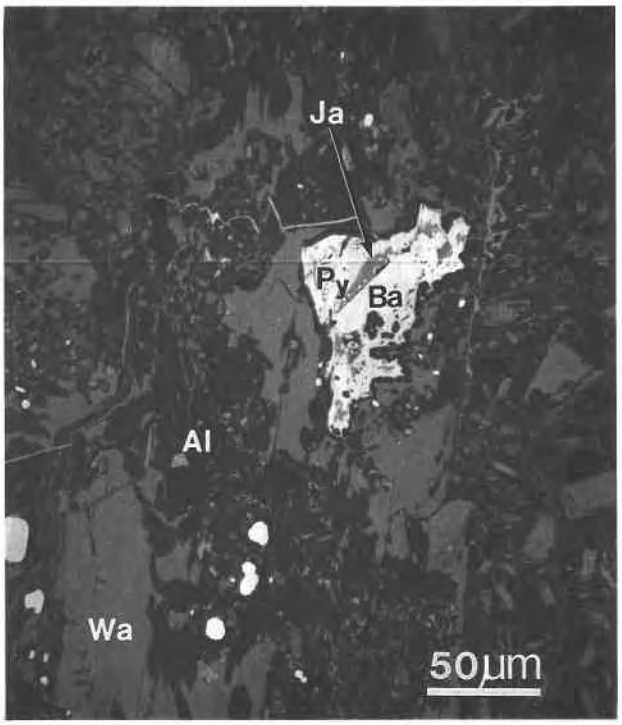

Fig. 1. Walthierite (Wa) associated with alunite (Al), barite (Ba), jarosite (Ja), and pyrite (Py), with the walthierite partially replaced by alunite. SEM BSE image.

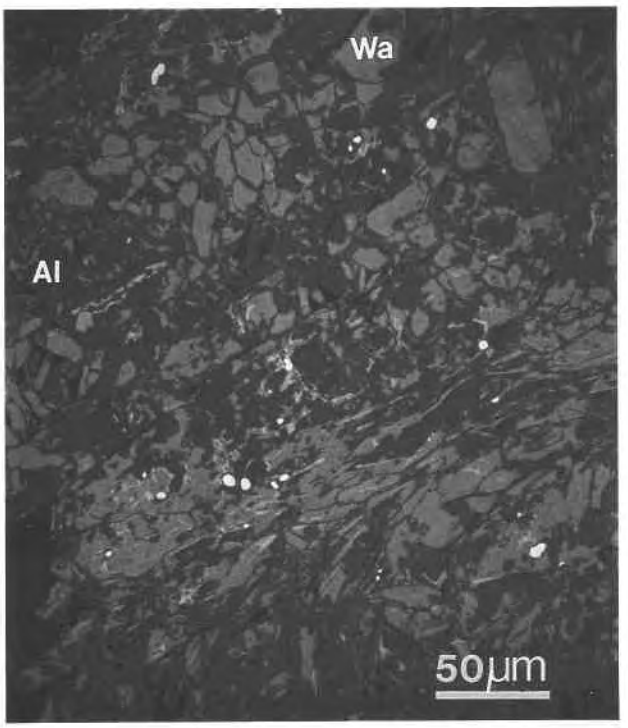

Fig. 2. Subhedral and euhedral walthierite enclosed within alunite. There are elongated walthierite and alunite grains in the lower portion of the figure, with some narrow wavy strips of walthierite within alunite. BSE image.

minamiite has been used for a Ca-bearing alunite group mineral, it has also been necessary to determine that the name does not represent end-member material. Both new minerals, their names, and the status of minamiite have been approved by the Commission on New Minerals and Mineral Names (CNMMN), International Mineralogical Association (IMA). Type materials for walthierite and huangite are deposited in the Smithsonian Institution under catalogue numbers NMNH 170208 and NMNH 170209, respectively.

Occurrences

Walthierite was found in the Reina vein in the Tambo mining district, which is approximately 7 km southeast of the El Indio gold, silver, and copper deposit, Coquimbo region, Chile. Two major hydrothermal assemblages fill open spaces in a fault at Reina. The earlier consists dominantly of barite, with subordinate pyrite, galena, electrum, and tennantite, whereas the latter comprises mostly alunite, with minor amounts of hematite, jarosite, scorodite, quartz, and Au. Fluid inclusion analyses indicate that barite and alunite formed from solutions with salinities of less than 1 *m* NaCl equivalent at temperatures of 175–275 °C (B. Ahler, personal communication, 1988). Wall rocks cut by the fault are pyroclastic rhyolites and a quartz monzonite porphyry that have undergone intense leaching, with preservation only of quartz phenocrysts. Textural relations indicate that alunite formed in wall rocks contemporaneously with the deposition of vein barite and that alunite formation utilized original K and Al with introduced sulfates. Walthierite is intimately associated with alunite, barite, quartz, pyrite, and jarosite within the vein (Fig. 1). The alunite + barite + quartz assemblage in this district is considered to be related to Au mineralization (Walthier et al., 1985).

In thin section, walthierite is colorless, granular, or tabular in habit. It occurs as subhedral to anhedral crystals ranging from 5 to 100 μm in length in individual grains and as aggregates. As revealed by backscattered electron images (BSE), irregular and angular walthierite is usually surrounded and replaced by alunite, whereas euhedral walthierite is occasionally observed overgrown by alunite (Figs. 1, 2). Zones of intermediate composition occur between walthierite and alunite, as observed by SEM. In some areas, elongated walthierite and alunite grains occur in parallel groups, with some narrow wavy strips of walthierite within alunite (Fig. 2). Cracked grains of walthierite are common, with the space between displaced fragments having been filled by alunite.

Some walthierite aggregates are observed closely associated with and replacing barite. The size of barite grains varies from micrometers to millimeters. Most barite crystals have a rounded or irregular shape, and some are honeycomblike, showing a relict texture produced by replacement by walthierite or alunite. Some barite grains also show internal fractures. Textural relations suggest that

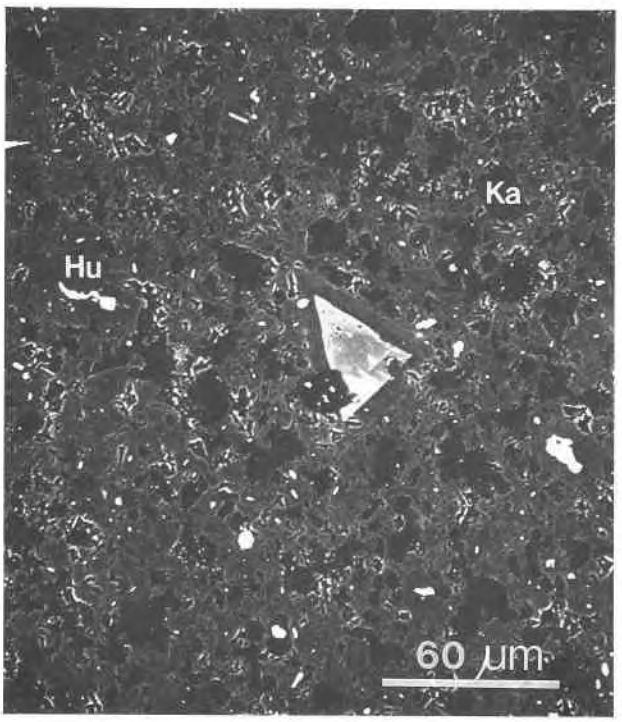

Fig. 3. A large huangite crystal (Hu) with a euhedral core consisting of woodhouseite, svanbergite, and hinsdalite solid solutions. The fine-grained matrix is huangite and kaolinite (Ka). BSE image.

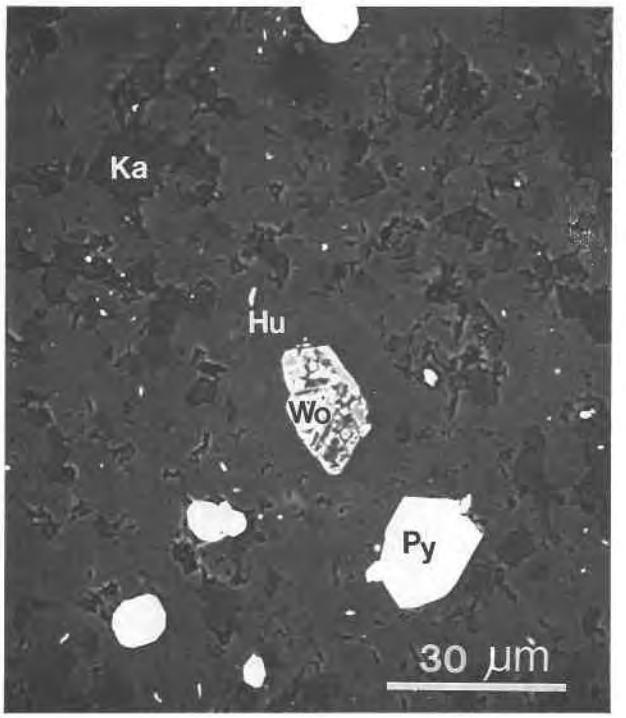

Fig. 4. Subhedral huangite crystal with a core of woodhouseite (Wo). The very bright crystals are pyrite (Py). BSE image.

barite formed earliest; the reaction of barite with fluids gave rise to walthierite, which was then fragmented and deformed. Finally, a K-rich hydrothermal fluid was introduced, resulting in the formation of alunite, in part through the replacement of walthierite.

Huangite was found in the El Indio deposit in the Campana B vein. This area has been affected by complex hydrothermal solutions in the late stages of development of an acid volcanic caldera during the Tertiary. The Campana vein cuts rhyolitic tuffs and is filled with coarse euhedral enargite, pyrite, and alunite. The sulfides are not contemporaneous with the alunite nor are they in isotopic equilibrium (Jannas et al., 1990). Wall rocks to the vein are altered to a mixture of kaolinite, alunite, and pyrite, with lesser pyrophyllite and sericite, and occasional minamiite and woodhouseite. Huangite occurs enclosed in and apparently equilibrated with kaolinite. Quartz is occasionally found in the vein but is accompanied by kaolinite only in wall rocks. Fluid inclusion studies indicate that the vein formed at temperatures of 225–275 °C with fluid salinities of ca. 0.6 *m* NaCl equivalent.

In polished thin section, huangite, which occurs as anhedral to subhedral crystals typically 3–10 μm in diameter, is the predominant mineral and is associated with kaolinite and pyrite. Rounded aggregates up to 20 μm in diameter are common and are surrounded by kaolinite aggregates of the same size (Fig. 3). In plane-polarized light, larger huangite grains (up to 40–70 μm in length) are also observed, but without exception they show a turbid core, with the clear huangite rims being only 3–8 μm thick. The turbid cores and rims of huangite grains vary in shape from euhedral to anhedral (Figs. 3, 4). In some instances, the turbid core materials have been cracked and individual fragments displaced. They have been overgrown or partially replaced by huangite, with resultant well-defined zoning. The turbid materials were determined by qualitative energy dispersive spectrometry analyses (EDS) and quantitative wavelength dispersive spectrometry analyses (WDS) to be solid solutions of the woodhouseite subgroup. The turbid cores may be divided into four compositional zones by contrast in BSE images and by EDS analysis. One or more zones may be absent; however, the outermost zone (zone 1 in Table 1), which is the most Ca-rich phase, occurs commonly.

Physical and optical properties

Both walthierite and huangite are white to yellowish in color, with white streak, glassy luster, and a perfect and easily produced {001} cleavage. The densities could not be measured because of the small grain sizes and the ubiquitous presence of other adhering minerals. Calculated densities are 3.02 g/cm^3 for walthierite and 2.80 g/cm^3 for huangite. Optically, both walthierite and huangite are uniaxial positive, elongation negative. No pleochroism was observed. The indices of refraction in white light are ω = 1.588(2), ϵ = 1.604(2) for walthierite. Cal-

TABLE 1. Electron microprobe analyses (in weight percent) of walthierite, huangite, and woodhouseite solid solutions

	Wal-thierite	Huang-ite	Core* of woodhouseite$_{ss}$			
			Zone 1	Zone 2	Zone 3	Core
Na_2O	0.28	0.43	0.41	0.52	0.50	0.46
K_2O	0.42	0.67	0.74	0.52	0.70	0.65
CaO	0.07	6.17	6.95	3.22	3.46	3.53
BaO	16.17	0.13	1.95	4.37	6.34	5.43
PbO	—	—	0.09	8.94	5.12	5.24
SrO	0.04	0.04	1.33	2.87	3.30	3.24
Fe_2O_3	0.05	0.10	0.17	0.11	—	0.07
Al_2O_3	33.65	38.62	36.82	32.07	34.42	34.85
P_2O_5	0.03	0.23	9.84	9.79	9.91	10.51
SO_3	34.59	38.78	24.81	21.24	21.60	21.45
F	0.03	0.11	0.14	0.14	0.18	0.28
H_2O**	11.89	13.60	13.21	11.69	12.03	12.05
−O = F	0.01	0.05	0.07	0.07	0.09	0.14
Total	97.21	98.83	96.39	95.41	97.47	97.71
Number of atoms based on 3(Al + Fe^{3+})						
Na	0.04	0.06	0.06	0.08	0.07	0.07
K	0.04	0.06	0.07	0.05	0.07	0.06
Ca	0.01	0.44	0.51	0.27	0.27	0.28
Ba	0.48	—	0.05	0.14	0.18	0.16
Sr	—	—	0.05	0.13	0.14	0.14
Pb	—	—	—	0.19	0.10	0.10
Fe^{3+}	—	0.01	0.01	0.01	—	—
Al	3.00	2.99	2.99	2.99	3.00	3.00
P	—	0.01	0.57	0.66	0.62	0.65
S	1.96	1.92	1.28	1.26	1.20	1.17
F	0.01	0.02	0.03	0.04	0.04	0.07
Mol% of alunite and woodhouseite group end-members†						
Na	4	6	8	9	8	8
Al	4	6	9	5	8	7
Wa	90	—	—	—	—	—
Hu	2	87	10	15	16	7
Wo	—	1	60	22	22	30
Ba-Wo	—	—	6	15	20	19
Sv	—	—	6	14	16	17
Hi	—	—	—	20	11	12

* The sequence of analyses from the center of the core outward is core, zone 3, zone 2, then zone 1; ss = solid solution.

** Calculated on the basis of 6(OH,F) per formula unit.

† Na = natroalunite $NaAl_3(SO_4)_2(OH)_6$; Al = alunite $KAl_3(SO_4)_2(OH)_6$; Wa = walthierite; Hu = huangite; Wo = woodhouseite $CaAl_3(SO_4)(PO_4)(OH)_6$; Ba-Wo = $BaAl_3(SO_4)(PO_4)(OH)_6$; Hi = hinsdalite $PbAl_3(SO_4)(PO_4)(OH)_6$; Sv = svanbergite $SrAl_3(SO_4)(PO_4)(OH)_6$.

culation of the compatibility index (Mandarino, 1981) yields a value of 0.046, which is appropriate for walthierite using the observed composition, the calculated density, and the observed indices of refraction. No indices of refraction could be measured for huangite because of its small grain size.

CHEMICAL COMPOSITIONS

A Cameca Camebax electron microprobe analyzer (EMPA) was utilized to determine the chemical compositions of walthierite and huangite by WDS. Various operating conditions were investigated in order to avoid volatilization of alkalis and to minimize thermal damage to the samples. Final operating conditions for walthierite and huangite, respectively, included accelerating voltages of 12 and 10 kV and beam currents of 5 and 4 nA, with scanning over an area 3–6 μm square for both minerals. A counting time of 30 s was used for all elements, except K and Na, for which we counted 15 s, in order to minimize diffusion of those elements, and F, for which we counted a time of 60 s. The standards used for analysis were Tiburon albite (Na), Gotthard adularia (K), andalusite (Al), synthetic ferrosilite (Fe), anhydrite (Ca), barite (Ba), celestite (Sr,S), Evans apatite (F,P), and galena (Pb). H_2O was not determined directly because of the paucity of materials. However, the calculated H_2O content is implied by the isostructural relations of both walthierite and huangite with alunite. The low analytical totals are correlated with sample damage during electron microprobe analysis, but cation ratios appear to be unaffected by this problem.

Those analyses with totals that were unreasonably low were discarded, with the assumption that they were adversely affected by beam damage. The analytical data for walthierite, as determined from six electron microprobe analyses, and those for huangite, averaged from seven analyses, together with four representative analyses for the different zones of the turbid core materials, are given in Table 1. The compositions, calculated on the basis of 3(Al + Fe^{3+}), are $(Ba_{0.48}Na_{0.04}K_{0.04}Ca_{0.01}\square_{0.43})Al_{3.00}S_{1.96}O_{7.91}[(OH)_{5.99}F_{0.01}]$ and $(Ca_{0.44}Na_{0.06}K_{0.06}\square_{0.44})(Al_{2.99}Fe^{3+}_{0.01})(S_{1.92}P_{0.01})O_{7.77}[(OH)_{5.98}F_{0.02}]$ for walthierite and huangite, respectively. They are idealized as $Ba_{0.5}\square_{0.5}Al_3(SO_4)_2(OH)_6$ and $Ca_{0.5}\square_{0.5}Al_3(SO_4)_2(OH)_6$ with $Z = 6$. The form of the formulae is consistent with that of alunite, $KAl_3(SO_4)_2(OH)_6$, with 0.5 vacancies in the 12-fold-coordinated M site, as required for charge balance caused by substitution of divalent Ba^{2+} or Ca^{2+} for monovalent K^+.

Significant chemical variation occurs in walthierite and is revealed by contrast in BSE images. In addition to the nearly ideal Ba end-member described above, phases intermediate in composition between walthierite and alunite were detected by qualitative EDS and quantitative WDS analyses within the overgrowth zones of walthierite by alunite; e.g., some quantitative WDS analyses yielded compositions with Ba/K = 3/4, corresponding to 40 mol% alunite in walthierite. Up to 15 mol% walthierite has been found in alunite coexisting with walthierite (Fig. 5a). Significant chemical variation was also detected in some huangite grains, for which the Ca/(K + Na) ratio ranged from 3/4 to 2/1 (Fig. 5b). Materials of complex compositions were found in the turbid cores of huangite, with significant variations detected in Ca, Sr, Pb, Ba, Na, and K in the 12-fold-coordinated site, and significant variations, in PO_4^{3-} (0.5–0.8 per formula unit, Table 1). This implies that the turbid material is composed of solid solutions among alunite and woodhouseite subgroup minerals, in which half of the SO_4^{2-} in the alunite structure is replaced by PO_4^{3-}, and the 12-fold-coordinated M site is occupied by divalent cations to maintain charge balance, giving rise to phases such as woodhouseite (Ca end-member), svanbergite (Sr end-member), and hinsdalite (Pb end-member).

Crystallographic data

The crystals of huangite were too small to allow separation from thin sections for standard X-ray diffraction studies. In addition, the crystals of walthierite were exceptionally small, giving rise to weak diffraction patterns. Single-crystal diffraction data were therefore obtained by electron diffraction. Ion-milled transmission electron microscope (TEM) samples were prepared from thin sections that were attached with sticky wax, utilizing areas that contained typical crystals of walthierite and huangite, as determined with optical and SEM observations, including both BSE images and EDS analyses. A Philips CM12 scanning transmission electron microscope (STEM), fitted with a Kevex Quantum detector for EDS analysis, was utilized for TEM studies. Crystals from which selected area electron diffraction (SAED) data were obtained were first characterized by qualitative chemical analysis and standard imaging techniques. Crystals of each mineral were identified in the TEM, in part by using semiquantitative EDS analyses, all such analyses being in agreement with separate EMPA analyses.

The SAED data for both walthierite and huangite are consistent with data for other members of the alunite group, with extinctions consistent with space groups $R3m$, $R32$, or $R\bar{3}m$ and lattice parameters observed to be a = 7.08 Å, c = 17.18 Å for walthierite, a = 6.95 Å, c = 16.97 Å for huangite, and a = 7.02 Å, c = 17.28 Å for alunite coexisting with walthierite; however, as shown below, powder XRD data showed that the values of c for walthierite and huangite are double those values. The space group is assumed to be $R\bar{3}m$ for both minerals by analogy with alunite (space group $R\bar{3}m$, Wang et al., 1965; Menchetti and Sabelli, 1976; a = 6.982 Å, c = 17.32 Å, Bayliss et al., 1986).

Powder X-ray diffraction data were obtained utilizing a Gandolfi camera 114.6 mm in diameter and a few small grains of walthierite, Cu$K\alpha$ (Ni-filtered) radiation, and quartz as an internal standard. Data for huangite were obtained using an automated Philips X-ray diffractometer with a graphite monochrometer and Cu$K\alpha$ radiation with quartz as an internal standard. A powdered whole-rock sample that had been shown by optical and SEM studies to consist largely of huangite but containing small amounts of other minerals was used. However, peaks of all phases except those of other members of the alunite group were easily identified and avoided. Because the other associated members of the alunite group constituted only a small portion of the specimen, their contribution was not significant, as verified by the presence of sharp, single symmetrical peaks, even at high 2θ values. No peaks from other phases were detected in patterns of walthierite.

Powder diffraction data are listed in Table 2, with data for alunite for comparison. Peaks with $d \approx 11$ Å for walthierite and huangite could be indexed only by doubling the values of c that were obtained by electron diffraction.

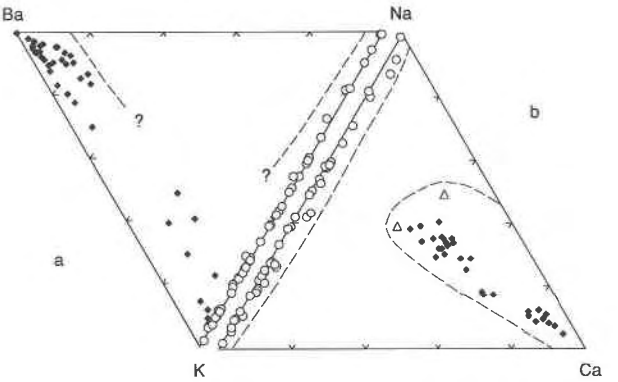

Fig. 5. Plot of compositions of natural alunites: open circles = King (1953), Moss (1958), Parker (1962), Slansky (1975), Wise (1975), Goldbery (1978, 1980), Huang and Chang (1982); open triangles = Ossaka et al. (1982, 1987); closed diamonds = this paper. (**a**) Plot in terms of components Ba-Na-K; (**b**) plot in terms of components Na-K-Ca.

Such peaks have been observed to be the most intense of those with l odd in powder XRD patterns of phases for which c is doubled (Okada et al., 1987; Ossaka et al., 1987). Because doubling is caused by the ordering of vacancies and M^{2+} cations on M sites, the inconsistency between electron diffraction and powder XRD data is inferred to be due to disorder induced by the electron beam, probably through specimen heating. Cell parameters were refined by least squares, giving rise to the values a = 6.992(4) Å, c = 34.443(8) Å for walthierite, which are slightly larger than a and smaller than c of synthetic $Ba_{0.5}Al_3(SO_4)_2(OH)_6$ [a = 6.9886(9) Å and c = 34.587(5) Å, Okada et al., 1987], and a = 6.983(4) Å and c = 33.517(9) Å for huangite, which are slightly larger than those of synthetic $Ca_{0.5}Al_3(SO_4)_2(OH)_6$ [a = 6.9751(6) Å and c = 33.415(3) Å, Ossaka et al., 1987] and minamiite [a = 6.981(2) Å and c = 33.490(14) Å, Ossaka et al., 1982]. These and other data collectively demonstrate that walthierite and huangite are isostructural with alunite. The superstructures of walthierite and huangite are probably caused by the ordering of Ba^{2+} or Ca^{2+} in M sites, as reported in plumbojarosite (Szymański, 1985) and minamiite (Ossaka et al., 1982). In contrast to the structure of alunite, in which only one M site exists, plumbojarosite and minamiite have two M sites, M1 and M2. The M1 and M2 sites in minamiite have average contents of $Na_{0.44}K_{0.20}\square_{0.36}$ and $Na_{0.28}Ca_{0.54}\square_{0.18}$, respectively (Ossaka et al., 1982). Most or all of the M^{2+} cations in walthierite and huangite probably occupy M2 with vacancies on M1, by analogy with plumbojarosite, in which Pb^{2+} occupies 96% of the M2 site (Szymański, 1985).

The magnitude of c has been shown to vary with the radius of the large cations in the 12-fold-coordinated site (Parker, 1962; Botinelly, 1976; Menchetti and Sabelli, 1976; Shannon, 1976; Huang and Chang, 1982; Altaner et al., 1988), e.g., c = 16.75 Å for natroalunite (Menchetti

TABLE 2. X-ray powder diffraction data for walthierite and huangite compared with alunite

	Walthierite			Huangite			Alunite**		
hkl	d_{obs}	d_{calc}	I/I_0*	d_{obs}	d_{calc}	I/I_0	*hkl*	*d*	I/I_0
003	11.50	11.48	10	11.09	11.17	10	—	—	—
006	5.73	5.74	50	5.57	5.59	11	003	5.77	30
102	—	—	—	5.66†	5.69†	13†	101	5.72	14
014	4.97	4.95	45	4.91	4.90	75	012	4.96	55
110	3.49	3.50	55	3.49	3.49	31	110	3.49	20
116	2.98	2.99	100	2.97	2.96	100	113	2.99	100
0,0,12	2.87	2.87	10	2.79	2.79	22	006	2.89	100?
028	—	—	—	2.455	2.452	35	024	2.477	6
1,0,14	2.283	2.279	80	2.231	2.226	51	107	2.293	80
124	2.217	2.212	30	—	—	—	122	2.211	6
0,1,16	2.029	2.028	8	1.979	1.979	21	018	2.038	2
218	—	—	—	—	—	—	214	2.022	2
0,0,18	1.909	1.914	70	1.864	1.862	19	009	1.926	70
306	—	—	—	1.899†	1.896†	43†	303	1.903	30
2,0,16	—	—	—	—	—	—	208	1.762	2
220	1.747	1.748	60	1.745	1.746	37	220	1.746	16
1,1,18	1.682	1.679	2	1.646	1.643	19	119	1.684	2
314	1.648	1.648	2	—	—	—	312	1.648	2
318	—	—	—	1.558	1.557	15	—	—	—
3,1,10	1.503	1.510	40	—	—	—	315	1.509	4
0,2,20	—	—	—	1.468	1.466	26	0,2,10	1.503	35
2,2,12	—	—	—	—	—	—	226	1.494	10
408	1.429	1.428	8	—	—	—			
0,3,18	1.390	1.389	20	—	—	—			
3,1,14	—	—	—	1.375	1.374	40			
3,1,16	1.322	1.324	4	—	—	—			
410	—	—	—	1.321	1.320	17			
2,2,18	1.289	1.291	10	1.270	1.274	14			
3,2,14	1.212	1.210	21	—	—	—			
3,1,20	—	—	—	1.184	1.186	15			
2,3,16	1.168	1.167	8						
5,0,10	1.143	1.143	8						

Note: The question mark indicates questionable intensity.
* Intensities estimated visually.
** Bayliss et al. (1986).
† Not in the sequence of decreasing *d* values in order to facilitate comparison with alunite.

and Sabelli, 1976) [$r(Na^+)$ = 0.97 Å]; c = 17.18 Å for hydronium alunite (Kubisz, 1970) [$r(H_3O^+)$ = 1.24 Å]; c = 17.32 Å for alunite [$r(K^+)$ = 1.33 Å]; c = 17.86 Å for ammonioalunite (Altaner et al., 1988) [$r(NH_4^+)$ = 1.43 Å]. When one takes the presence of vacancies in the 12-fold-coordinated M site into account, the $c/2$ values of walthierite [$c/2$ = 17.221(9) Å, $r(Ba^{2+})$ = 1.34 Å] and huangite [$c/2$ = 16.758(9) Å, $r(Ca^{2+})$ = 0.99 Å] are in good agreement with this relation. The magnitude of c has also been shown to vary with the radius of the M cations among synthetic materials with formula $M_{0.5}\square_{0.5}Al_3(SO_4)_2(OH)_6$, with M = Ca^{2+}, Sr^{2+}, Pb^{2+}, and Ba^{2+} (Okada et al., 1987).

Discussion

Status of minamiite

Minamiite was originally described as a Ca-rich member of the alunite group (Ossaka et al., 1982), and the name was used for synthetic $Ca_{0.5}\square_{0.5}Al_3(SO_4)_2(OH)_6$ (Ossaka et al., 1987). However, the M sites in the structure of type minamiite have a composition of $Na_{0.36}Ca_{0.27}K_{0.10}\square_{0.27}$. Nickel and Mandarino (1987) noted that end-member mineral species are defined only on the basis of the predominant component on a given site. Thus, even though the charge contributed by Ca^{2+} is the largest of all M-site cations in a minamiite, Na is still the dominant cation (Fig. 5b). The CNMMN, IMA, has therefore accorded huangite the status of a Ca end-member of the alunite group, as Ca is the dominant M-site cation in huangite. Minamiite is Na dominant, as is natroalunite, but differs from natroalunite in having c doubled (Mandarino, written communication, 1991).

Solid solutions and possible solvi

Although the coupled substitution of $SO_4^{2-} + M^+ = PO_4^{3-} + M^{2+}$ in alunite brings about woodhouseite group minerals having a ratio of S/P = 1, both groups have space group $R\bar{3}m$ and similar lattice parameters (Wang et al., 1965; Kato, 1971, 1977; Menchetti and Sabelli, 1976; Kato and Miura, 1977). Solid solutions occur for various M-site ions within the group, e.g., substitution of Na^+ for K^+ exists over the entire alunite-natroalunite system (Parker, 1962), and recent experimental studies by Stoffregen and Cygan (1990) demonstrate that alunite and natroalunite are completely miscible at 450 and 350 °C, but they do not rule out a solvus at 250 °C. Extensive substitution of K by other species such as NH_4^+ (Altaner et al., 1988), or H_3O^+ (Kubisz, 1970; Ripmeester et al.,

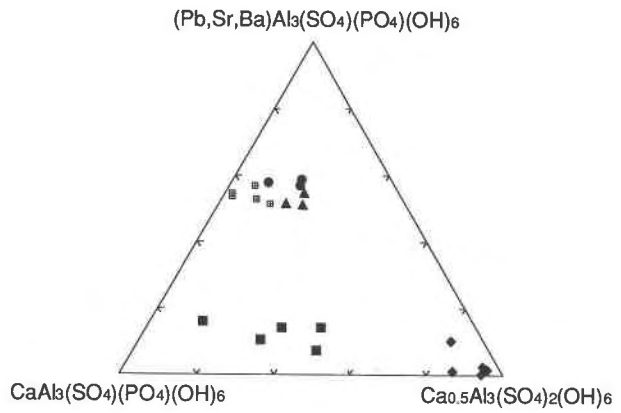

Fig. 6. A plot of compositions in the ternary system $(Pb,Sr,Ba)Al_3(SO_4)(PO_4)(OH)_6$-$CaAl_3(SO_4)(PO_4)(OH)_6$-$Ca_{0.5}Al_3(SO_4)_2(OH)_6$ showing solid solution between woodhouseite subgroup minerals and huangite; crossed squares = core of woodhouseite crystal; closed triangles = zone 3; closed circles = zone 2; closed squares = zone 1; closed diamonds = huangite.

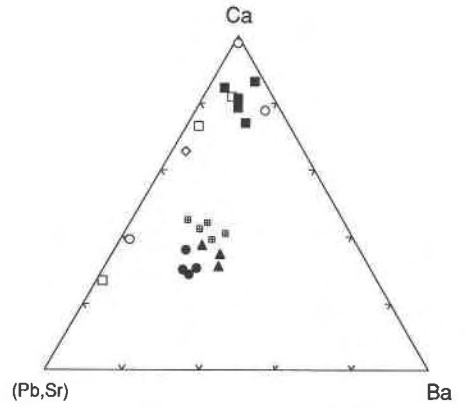

Fig. 7. Plot of compositions in the ternary system Ca-(Pb,Sr)-Ba for woodhouseite minerals. Open diamonds = Qin et al. (1983); open circles = Wise (1975); open squares = Stoffregen and Alpers (1987). Other symbols as in Figure 6.

1986) in alunite, and substitution of Sr^{2+} for Ca^{2+} in the woodhouseite-svanbergite system (Wise, 1975; Qin et al., 1983; Stoffregen and Alpers, 1987) also occur. Some solid solution also has been shown to occur between alunite and woodhouseite group minerals (Wise, 1975; Stoffregen and Alpers, 1987); this is not unexpected, in part because no ordering has been observed between SO_4^{2-} and PO_4^{3-} groups in woodhouseite minerals (Kato, 1971; Blount, 1974).

Figure 5 shows a wide range of compositions for natural alunite group minerals, including walthierite, huangite, alunite coexisting with walthierite, and intermediate phases between walthierite and alunite (this study), and other analyses from the literature. Figure 5a, which is a plot of analyses for the ternary Ba-K-Na system, shows that complete solid solution exists for the alunite-natroalunite series, and that it is probable for the walthierite-alunite system, for which ionic radii of M-site cations [$r(Ba^{2+}) = 1.34$ Å, $r(K^+) = 1.33$ Å] are similar. However, the available data show a gap for Ba ranging from 40 to 60% in the Ba-K series, and the four analyses with approximately 20–40% Ba must be interpreted cautiously, as they may represent mixtures between walthierite and alunite due to overlap during EMPA analysis (Fig. 5a). The paucity of phases with high K contents relative to Ba may be attributed to either a lack of naturally occurring solutions with compositions that could give rise to such phases or to a solvus, which would be complicated by order-disorder relations among phases with M^{2+} cations that may affect the form of solvi. In contrast, mutual solid solution between walthierite and natroalunite is very limited. The ordering of vacancies and M^{2+} cations in walthierite and the large difference in the radii of Ba^{2+} (r = 1.34 Å) and Na^+ (r = 0.97 Å) are consistent with an extensive miscibility gap between walthierite and natroalunite. A possible nonsymmetric solvus may be constrained at compositions of walthierite with less than 15 mol% of natroalunite and less than 5 mol% of walthierite in natroalunite in the absence of K, on the basis of our data; the range of mutual solid solution is expected to increase as K^+ content increases (Fig. 5a).

Huangite displays a continuous increase in Na^+ and K^+ contents up to 45 mol% of total natroalunite plus alunite components (Fig. 5b); nevertheless, the trend appears to have a ratio of Na/K > 1. The two minamiite compositions given by Ossaka et al. (1982, 1987) also have Na/K > 1, with $Na_{0.36}Ca_{0.27}K_{0.10}\square_{0.27}$ and $Na_{0.29}K_{0.25}Ca_{0.23}\square_{0.23}$ on the M sites per formula unit, respectively. These data collectively suggest that extensive solid solution between huangite and natroalunite is very likely. Nevertheless, the available data may be used to define a gap in composition in the Ca-Na series from 5 to approximately 50% Ca that may result from restrictions on the composition of formation fluids or a solvus that is related to ordered vacancies in Ca-rich phases. Similarly, a wide miscibility gap may exist between alunite and huangite (Fig. 5b). Ossaka et al. (1987) demonstrated that $Ca_{0.5}Al_3(SO_4)_2(OH)_6$ formed in solutions containing only Ca^{2+} and Na^+ but no K^+. Minamiite was found coexisting with large domains of alunite within one crystal (Ossaka et al., 1982). No alunite coexisting with huangite is found in this study, but such relations may have been restricted by compositions of formation fluids.

The compositional ranges of the turbid core materials in huangite are shown in Figures 6 and 7, with all data [(K + Na)/(K + Na + Ca + Ba + Pb + Sr) < 0.2] falling into the field of woodhouseite subgroup minerals. The turbid materials are complex combinations of various end-members such as woodhouseite, hinsdalite, svanbergite, huangite, natroalunite, and alunite, but without exception the woodhouseite end-member is predominant (Table 1). There is a trend of decreasing woodhouseite component from the core (30 mol%) outward to zone 2 (22 mol%); nevertheless, the outermost zone (zone 1) of the turbid core contains the greatest woodhouseite component (60

mol%), indicating that a Ca-rich fluid was introduced after the formation of the inner core. The trend is paralleled by an increase in the huangite component (up to 40 mol% in one analysis of zone 1) in woodhouseite, suggesting that intermediate members exist between huangite and woodhouseite.

Figure 7 shows compositional variation of the turbid core materials within the woodhouseite subgroup. There is an increase in Pb + Sr from grain centers to zone 2. Complete solid solution within woodhouseite minerals seems likely (Wise, 1975). It is noteworthy that compositions of the turbid cores show significant Ba contents (up to 0.2 Ba^{2+} per formula unit in zone 3; Table 1, Fig. 7). Others have observed Ba in woodhouseite. Wise (1975) found woodhouseite in metavolcanic rocks with 20 mol% Ba in the M site. Stoffregen and Alpers (1987) observed woodhouseite with up to 9.58 wt% BaO in one sample and solid solution between woodhouseite and svanbergite with some Ba. These data collectively suggest that another end-member of the woodhouseite subgroup, $BaAl_3[(SO_4)(PO_4)](OH)_6$, may occur naturally.

Phase equilibrium of alunite-group minerals

When equilibrated with quartz, alunite group minerals constrain the stabilities of micas:

$$\underset{\text{alunite}}{KAl_3(SO_4)_2(OH)_6} + 3SiO_2 = \underset{\text{muscovite}}{KAl_3Si_3O_{10}(OH)_2} + 2H_2O + \underset{\text{fluid}}{S_2} + 3O_2 \quad (1)$$

$$\underset{\text{natroalunite}}{NaAl_3(SO_4)_2(OH)_6} + 3SiO_2 = \underset{\text{paragonite}}{NaAl_3Si_3O_{10}(OH)_2} + 2H_2O + \underset{\text{fluid}}{S_2} + 3O_2 \quad (2)$$

$$\underset{\text{walthierite}}{2Ba_{0.5}Al_3(SO_4)_2(OH)_6} + 4SiO_2 = \underset{\text{barium mica}}{BaAl_4Si_2O_{10}(OH)_2} + \underset{\text{kaolinite}}{Al_2Si_2O_5(OH)_4} + 3H_2O + \underset{\text{fluid}}{2S_2} + 6O_2 \quad (3)$$

$$\underset{\text{huangite}}{2Ca_{0.5}Al_3(SO_4)_2(OH)_6} + 4SiO_2 = \underset{\text{margarite}}{CaAl_4Si_2O_{10}(OH)_2} + \underset{\text{kaolinite}}{Al_2Si_2O_5(OH)_4} + 3H_2O + \underset{\text{fluid}}{2S_2} + 6O_2. \quad (4)$$

Reaction 1 was calculated at 250 °C and at a pressure defined by vapor saturation by Jannas et al. (1990), who combined it with sulfide reactions to fix f_{S_2} and f_{O_2} of early Cu mineralization at El Indio. In the case of huangite and walthierite, the R^{2+}/Al ratio is different than that in the equivalent mica, and an additional phase must be added to accommodate the excess Al. Kaolinite was chosen because it is common in acid sulfate systems and is found with huangite, but other reactions should be considered if huangite or walthierite is stable up to temperatures of pyrophyllite stability.

Although similar to Reactions 1 and 2, Reactions 3 and 4 may not provide realistic limits on the stability of walthierite and huangite, as barium mica and margarite are not found in hydrothermal deposits. Alternative equilibria involving other alkaline-earth sulfates and kaolinite may provide more appropriate bounds:

$$\underset{\text{walthierite}}{4Ba_{0.5}Al_3(SO_4)_2(OH)_6} + \underset{\text{quartz}}{12SiO_2} = \underset{\text{kaolinite}}{6Al_2Si_2O_5(OH)_4} + \underset{\text{barite}}{2BaSO_4} + \underset{\text{fluid}}{3S_2} + 9O_2 \quad (5)$$

$$\underset{\text{huangite}}{4Ca_{0.5}Al_3(SO_4)_2(OH)_6} + \underset{\text{quartz}}{12SiO_2} = \underset{\text{kaolinite}}{6Al_2Si_2O_5(OH)_4} + \underset{\text{anhydrite}}{2CaSO_4} + \underset{\text{fluid}}{3S_2} + 9O_2. \quad (6)$$

Reactions 5 and 6 are related to associations of these alunite group minerals in their type localities, as huangite is intergrown with kaolinite at the El Indio mine, and walthierite is observed replacing barite in association with quartz at the Reina vein. Other reactions could be formed with huangite and low-temperature calcium aluminum silicates such as prehnite or zeolites, but this is a moot exercise in the absence of data that would allow calculation of actual phase equilibria.

Helgeson et al. (1978) listed thermodynamic data for alunite, and Stoffregen and Cygan (1990) calculated the thermodynamic properties of natroalunite consistent with their experiments and the data of Helgeson et al. on alunite. Use of these data allows calculations of Reactions 1 and 2 with an internally consistent data set, e.g., Figure 8 at 500 bars and 500 K (227 °C). Alunite or natroalunite and quartz have similar stability fields in the fields of hematite and pyrite at very oxidizing and sulfidizing conditions, which constrains muscovite and paragonite to less oxidizing and sulfidizing conditions (Fig. 8). The stability of quartz + alunite as a function of f_{S_2} and f_{O_2} has previously been presented (Jannas et al., 1990), but to the authors' knowledge that for quartz + natroalunite has not. The relative positions of the reactions shown in Figure 8 do not vary significantly over 300–600 K and 1–5000 bars. If in equilibrium, occurrences of alunite + quartz + pyrite fix the f_{O_2} and f_{S_2} to high values, i.e., unusual conditions except in acid sulfate systems where alunite group minerals are found. The quartz-saturated stability fields of huangite and walthierite will have a similar shape to those of alunite and natroalunite because the molar ratio of S_2 to O_2 in Reactions 1–6 is identical, but no data are yet available to constrain their positions.

Ionic equilibria involving the alunite group minerals should also be considered, as Reactions 1–4 can only provide limits in metasomatic rocks. Hemley et al. (1969)

calculated various ionic equilibria from their experiments on the stability of alunite, including

$$\underset{\text{muscovite}}{KAl_3Si_3O_{10}(OH)_2} + 4H^+ + \underset{\text{fluid}}{2SO_4^{2-}} = \underset{\text{alunite}}{KAl_3(SO_4)_2(OH)_6} + \underset{\text{fluid}}{3SiO_2\ (aq)} \quad (7)$$

$$\underset{\text{kaolinite}}{3Al_2Si_2O_5(OH)_4} + 2K^+ + \underset{\text{fluid}}{6H^+} + 4SO_4^{2-} = \underset{\text{alunite}}{2KAl_3(SO_4)_2(OH)_6} + \underset{\text{fluid}}{6SiO_2\ (aq)} + 3H_2O. \quad (8)$$

Reaction 8 was also calculated by Heald et al. (1987). Silica minerals can be dissolved under vigorous acid attack in acid-sulfate conditions to levels in excess of quartz saturation, and the remaining quartz at Reina may be relict from the wall rocks. Early barite is corroded by later alunite within the front zone (Fig. 1), consistent with the reaction

$$\underset{\text{barite}}{2BaSO_4} + 3Al^{3+} + \underset{\text{fluid}}{K^+} + 6H_2O = \underset{\text{alunite}}{KAl_3(SO_4)_2(OH)_6} + \underset{\text{fluid}}{2Ba^{2+}} + 6H^+. \quad (9)$$

Replacement of wall-rock flour within the fault breccia is evidenced by zircon and rutile enclosed by alunite that has filled open space, but the low abundances of these insoluble minerals in the veins suggests that most Al was introduced. Walthierite formed locally during replacement of barite by alunite, indicating a reaction such as

$$\underset{\text{barite}}{BaSO_4} + \underset{\text{alunite}}{2KAl_3(SO_4)_2(OH)_6} = \underset{\text{walthierite}}{2Ba_{0.5}Al_3(SO_4)_2(OH)_6} + \underset{\text{fluid}}{2K^+} + SO_4^{2-}. \quad (10)$$

Formation of walthierite rather than alunite was controlled by cation concentrations in the solution

$$\underset{\text{fluid}}{Ba^{2+}} + \underset{\text{alunite}}{2KAl_3(SO_4)_2(OH)_6} = \underset{\text{walthierite}}{2Ba_{0.5}Al_3(SO_4)_2(OH)_6} + \underset{\text{fluid}}{2K^+}. \quad (11)$$

The growth of walthierite during replacement of barite is probably related to locally high Ba/K ratios in solution.

Woodhouseite, minamiite, and huangite are the only Ca minerals reported from wall rocks and veins at El Indio. Stoffregen and Alpers (1987) considered woodhouseite and other phosphate-sulfate minerals to form by replacement of apatite under acid sulfate conditions. Such conditions are consistent with the formation of huangite and woodhouseite at El Indio, except that phosphate was leached and replaced by sulfate to form huangite. With acid sulfate alteration alone, apatite would be converted to anhydrite, with phosphate removal facilitated by association with H^+. Formation of huangite rather than anhydrite is promoted in the presence of kaolinite at acidic conditions:

$$\underset{\text{anhydrite}}{CaSO_4} + \underset{\text{kaolinite}}{3Al_2Si_2O_5(OH)_4} + \underset{\text{fluid}}{6H^+} + 3SO_4^{2-} = \underset{\text{huangite}}{2Ca_{0.5}Al_3(SO_4)_2(OH)_6} + \underset{\text{fluid}}{6SiO_2\ (aq)} + 3H_2O. \quad (12)$$

This reaction emphasizes the importance of acid sulfate conditions for the stability of huangite. With incomplete assemblages and unconstrained activities of relevant aqueous species, accurate estimation of the free energies of formation for walthierite and huangite is presently prohibited in the known parageneses.

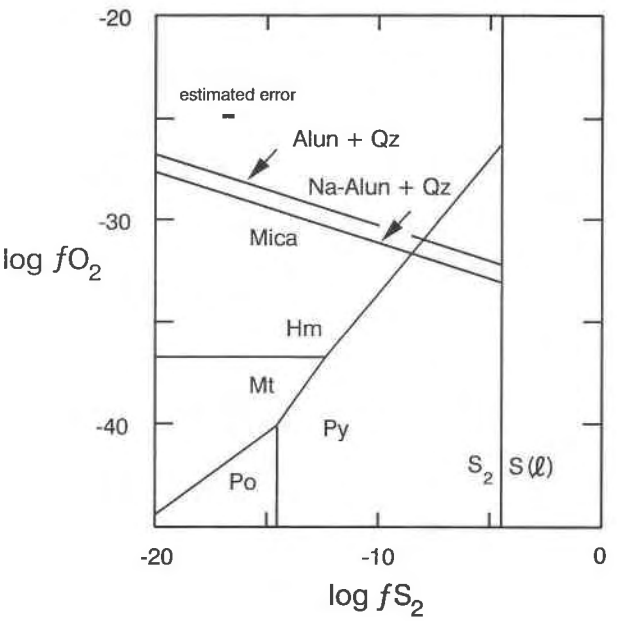

Fig. 8. Diagram of $\log_{10} f_{O_2}$ vs. $\log_{10} f_{S_2}$ at 500 K and 500 bars for Reactions 1 and 2 in comparison with equilibria for the system Fe-S-O. The calculated error brackets are based on ±10 kJ/mol for alunite and natroalunite (Stoffregen and Cygan, 1990). Thermodynamic data for alunite, micas, and quartz are from Helgeson et al. (1978), except for the volume for alunite (which has a factor of 2 error), for natroalunite from Stoffregen and Cygan (1990), and for Fe-S-O phases and the volume of alunite from Robie et al. (1978). Troilite activity in pyrrhotite coexisting with pyrite is taken as 0.5, and the vaporization of liquid S has been corrected for pressure (Craig and Scott, 1976). Hm = hematite, Mt = magnetite, Py = Pyrite, Po = pyrrhotite, S_2 = diatomic S (ideal gas), S (l) = liquid S, Alun = alunite, Na-Alun = natroalunite, Qz = quartz.

Acknowledgments

We gratefully acknowledge A. Arribas and Wei-Teh Jiang for valuable discussions and J.D. Grice and G. Ansell for their helpful and careful reviews. We thank M.A. Cosca for drafting one of the diagrams. The assistance of Carl E. Henderson in the use of the electron microprobe at

the University of Michigan Electron Microbeam Analysis Laboratory is greatly appreciated. The microprobe used in this study was acquired under grant no. EAR-8212764, the analytical SEM under grant no. BSR-83-14092, and the STEM under grant no. EAR-8708276 from the National Science Foundation. Contribution no. 484 from the Mineralogical Laboratory, Department of Geological Sciences, University of Michigan.

References cited

Altaner, S.P., Fitzpatrick, J.J., Krohn, M.D., Bethke, P.M., Hayba, D.O., Goss, J.A., and Brown, Z.A. (1988) Ammonium in alunites. American Mineralogist, 73, 145–152.

Bayliss, P., Erd, D.C., Mrose, M.E., Sabina, A.P., and Smith, D.K. (1986) Mineral powder diffraction file, p. 29. International Centre for Diffraction Data, Swarthmore, Pennsylvania.

Blount, A.M. (1974) The crystal structure of crandallite. American Mineralogist, 59, 41–47.

Botinelly, T. (1976) A review of the minerals of the alunite-jarosite, beudantite and plumbogummite groups. Journal of Research of the U.S. Geological Survey, 4, 213–216.

Craig, J.R., and Scott, S.D. (1976) Sulfide phase equilibria. In Mineralogical Society of America Reviews in Mineralogy, 1, 1–110.

Goldbery, R. (1978) Early diagenetic, non-hydrothermal Na-alunite in Jurassic flint clays, Makhtesh Raman, Israel. Geological Society of America Bulletin, 89, 687–698.

——— (1980) Early diagenetic Na-alunites in Miocene algal mat intertidal facies, Ras Sudar, Sinai. Sedimentology, 27, 189–198.

Heald, P., Foley, N.K., and Hayba, D.O. (1987) Comparative anatomy of volcanic-hosted epithermal deposits: Acid-sulfate and adularia-sericite types. Economic Geology, 82, 1–26.

Helgeson, H.C., Delany, J.M., Nesbitt, H.W., and Bird, D.K. (1978) Summary and critique of the thermodynamic properties of rock-forming minerals. American Journal of Science, 287A, 1–229.

Hemley, J.J., Hostetler, P.B., Gude, A.J., and Mountjoy, W.T. (1969) Some stability relations of alunite. Economic Geology, 64, 599–612.

Huang, C.K., and Chang, Y.H. (1982) Barite and alunite from the Chinkuashih gold-copper deposits, Taiwan. Acta Geologica Taiwanica, 21, 1–13.

Jannas, R.R., Beane, R.E., Ahler, B.A., and Brosnahan, D.R. (1990) Gold and copper mineralization at the El Indio deposit, Chile, Journal of Geochemical Exploration, 36, 233–266.

Kato, T. (1971) The crystal structures of goyazite and woodhouseite. Neues Jahrbuch für Mineralogie Monatshefte, 241–247.

——— (1977) Further refinement of the woodhouseite structure. Neues Jahrbuch für Mineralogie Monatshefte, 54–58.

Kato, T., and Miura, Y. (1977) The crystal structures of jarosite and svanbergite. Mineralogical Journal (Japan), 8, 419–430.

King, D. (1953) Origin of alunite deposits at Pidinga, South Australia. Economic Geology, 48, 689–703.

Kubisz, J. (1970) Studies on synthetic alkali-hydronium jarosites. I. Synthesis of jarosite and natrojarosite. Mineralogia Polonica, 1, 47–58.

Mandarino, J.A. (1981) The Gladstone-Dale relationship: Part IV: The compatibility and its application. Canadian Mineralogist, 19, 441–450.

Menchetti, S., and Sabelli, C. (1976) Crystal chemistry of the alunite series: Crystal structure refinement of alunite and synthetic jarosite. Neues Jahrbuch für Mineralogie Monatshefte, 9, 406–417.

Moss, A.A. (1958) Alumian and natroalunite. Mineralogical Magazine, 31, 884–885.

Nickel, E.H., and Mandarino, J.A. (1987) Procedures involving the IMA Commission on New Minerals and Mineral Names and guidelines on mineral nomenclature. Canadian Mineralogist, 25, 353–377.

Okada, K., Soga, H., Ossaka, J., and Otsuka, N. (1987) Syntheses of minamiite type compounds, $M_{0.5}Al_3(SO_4)_2(OH)_6$ with $M = Sr^{2+}$, Pb^{2+} and Ba^{2+}. Neues Jahrbuch für Mineralogie Monatshefte, 64–70.

Ossaka, J., Hirabayashi, J.-I., Okada, K., and Kobayashi, R. (1982) Crystal structure of minamiite, a new mineral of the alunite group. American Mineralogist, 67, 114–119.

Ossaka, J., Otsuka, N., Hirabayashi, J.-I., Okada, K., and Soga, H. (1987) Synthesis of minamiite, $Ca_{0.5}Al_3(SO_4)_2(OH)_6$. Neues Jahrbuch für Mineralogie Monatshefte, 49–63.

Parker, R.L. (1962) Isomorphous substitution in natural and synthetic alunite. American Mineralogist, 47, 127–136.

Qin, S., Sheng, J., Liu, J., and Guo, L. (1983) Strontium woodhouseite—An intermediate mineral between svanbergite and woodhouseite. Bulletin, Institute of Mineral Deposits, Chinese Academy of Geological Sciences, 1, 120–125 (in Chinese).

Ripmeester, J.A., Ratcliffe, C.I., Dutrizac, J.E., and Jambor, J.L. (1986) Hydronium ion in the alunite-jarosite group. Canadian Mineralogist, 24, 435–447.

Robie, R.A., Hemingway, R.S., and Fisher, J.R. (1978) Thermodynamic properties of minerals and related substances at 298.15 K and 1 bar (10^5 Pascals) pressure and higher temperatures. U.S. Geological Survey Bulletin, 1452, 1–456.

Shannon, W.D. (1976) Revised effective ionic radii and systematic studies of interatomic distances in halides and chalcogenides. Acta Crystallographica, A32, 751–767.

Slansky, E. (1975) Natroalunite and alunite from White Island Volcano, Bay of Plenty, New Zealand. New Zealand Journal of Geology and Geophysics, 18, 285–293.

Stoffregen, R.E., and Alpers, C.N. (1987) Woodhouseite and svanbergite in hydrothermal ore deposits: Products of apatite destruction during advanced argillic alteration. Canadian Mineralogist, 25, 201–211.

Stoffregen, R.E., and Cygan, G.L. (1990) An experimental study of Na-K exchange between alunite and aqueous sulfate solutions. American Mineralogist, 75, 209–220.

Szymański, J.T. (1985) The crystal structure of plumbojarosite, $Pb[Fe_3(SO_4)_2(OH)_6]_2$. Canadian Mineralogist, 23, 659–668.

Walthier, T.N., Sirvas, E., and Araneda, R. (1985) The El Indio gold, silver, copper deposit. Engineering and Mining Journal, 186(10), 38–42.

Wang, R., Bradley, W.F., and Steinfink, H. (1965) The crystal structure of alunite. Acta Crystallographica, 18, 249–252.

Wise, W.S. (1975) Solid solution between the alunite, woodhouseite, and crandallite mineral series. Neues Jahrbuch für Mineralogie Monatshefte, 12, 540–545.

Manuscript received October 28, 1991
Manuscript accepted July 16, 1992